Lithium–Sulfur Batteries

DOI: 10.1002/anie.201301250

Highly Reversible Lithium/Dissolved Polysulfide Batteries with Carbon Nanotube Electrodes**

*Yongzhu Fu, Yu-Sheng Su, and Arumugam Manthiram**

Rechargeable lithium–sulfur (Li–S) batteries are one of the most promising electrochemical energy storage devices that could provide a leap in specific energy over conventional lithium-ion (Li-ion) batteries.[1] Sulfur can theoretically accept $2e^-$ per atom leading to a capacity of 1675 $mAh\,g^{-1}$, which is an order of magnitude higher than that of conventional cathode materials (i.e., $LiCoO_2$, $LiMn_2O_4$, and $LiFePO_4$). A typical Li–S cell is composed of a Li metal anode, a non-aqueous electrolyte, and a solid sulfur composite cathode consisting of sulfur powder, conductive carbon, and a polymer binder. Sulfur undergoes a series of morphological and structural changes during the charge-discharge process involving the redox reaction ($S + 2Li^+ + 2e^- \leftrightarrow Li_2S$). While the elemental octasulfur (S_8) and the fully discharged product Li_2S are insoluble in the organic liquid electrolyte, the intermediate polysulfides (e.g., Li_2S_x, $x = 3$, 4, 6, and 8) formed during cycling are soluble in the electrolyte.[2] The dissolved polysulfides could shuttle between the anode and cathode during cycling, resulting in low Coulombic efficiency and severe capacity fade.[3] In addition, complete conversion of S_8 to Li_2S may not occur owing to the sluggish reaction kinetics involved in the transition of dissolved polysulfides to insoluble Li_2S. Also, the deposition of insulating Li_2S results in electrode passivation and an early ending of discharge, resulting in an incomplete end product Li_2S_2.[4]

Early investigations on Li–S batteries demonstrated only a partial formation of Li_2S_2/Li_2S in the cathode, with a reversible capacity of 500–800 $mAh\,g^{-1}$ corresponding to the utilization of less than $1.0e^-$ per sulfur atom.[5] Recent work on cleverly designed sulfur–carbon composites with improved structures and cell configurations that can effectively trap the polysulfides within the cathodes have shown reversible capacities in the range of 800–1200 $mAh\,g^{-1}$, allowing for reversible utilization of up to $1.3e^-$ per sulfur atom.[6] In 1979 Rauh et al. reported a Li/dissolved sulfur battery in which a dissolved polysulfide (Li_2S_n, $n \geq 8$) electrolyte was used as the catholyte with a Teflon-bonded carbon electrode.[2a] Over $1.6e^-$ per sulfur atom was utilized during the initial discharge at 50 °C at low rates (< C/10), but the efficiency deteriorated after 10–20 cycles. Recent studies on Li/dissolved sulfur cells also show promising results.[7] Although these results indicate that dissolved polysulfides could facilitate efficient electrochemical utilization of sulfur, longer cycle life and stable discharge capacities during cycling need to be demonstrated to embark on this approach. One shortcoming with the Li/dissolved sulfur system is that the volumetric energy density is low as indicated by Ji and Nazar.[1b] However, the liquid cathode is appealing to achieve high reaction activity in comparison to solid sulfur electrodes and could help enhance our understanding of the Li–S system.

Herein, we demonstrate a highly reversible Li/dissolved polysulfide cell utilizing a self-weaving, free-standing multi-walled carbon nanotube (MWCNT) "paper" as an electrode (Figure 1a). The MWCNT paper (Figure S1, Supporting information) was prepared by a dispersion–filtration process. The self-weaving behavior is frequently observed with different types of commercial single-walled, double-walled, and multi-walled CNTs, and this fabrication method has been utilized for preparing CNT electrodes for Li-ion batteries.[8] The polysulfide catholytes contain 1–3 M sulfur with a nominal molecular formula of Li_2S_6 in 1 M $LiCF_3SO_3$ and 0.1 M $LiNO_3$ in dimethoxy ethane (DME), and 1,3-dioxolane (DOL) (1:1 v/v). 40 μL of polysulfide catholyte was injected into the MWCNT paper on the cathode side. The cell with an open circuit voltage (OCV) of approximately 2.28 V was initially charged to 3.0 V followed by full discharge and charge in the voltage range of 3.0–1.8 V (Figure 1b). During the 1st charge, a single voltage plateau is seen, which corresponds to the process of oxidation of S_6^{2-} to high-order polysulfides (Li_2S_n, $n \geq 8$) or elemental sulfur. Two plateaus can be observed during the 1st discharge, which resemble the discharge profile of conventional Li–S cells (Figure S2), indicating that the 1st charge process converts polysulfides in the catholyte to an electrochemical state that is close to that of elemental sulfur. The subsequent charge shows the characteristic charge voltage plateaus of Li–S batteries.

Figure 1c shows a SEM image of the discharged MWCNT electrode. The porous MWCNT network is filled with discharged products and lithium salts, and that sulfur is uniformly distributed, as indicated by the elemental mapping (Figure S3). The electrode was washed by DME/DOL (1:1 v/v) solvent thoroughly to remove the soluble components. A representative microsized particle, which is completely wrapped by carbon nanotubes and embedded within the MWCNT network, is seen in the SEM image in Figure 1d and STEM image in Figure 1e. Low magnification STEM images reveal that similar particles are dispersed within both the charged and discharged MWCNT electrodes as shown, respectively, in Figure 1f and g. The XRD pattern (Figure 1h) of the pristine

[*] Dr. Y. Fu, Y.-S. Su, Prof. A. Manthiram
Materials Science and Engineering Program
Texas Materials Institute, The University of Texas at Austin
Austin, TX 78712 (USA)
E-mail: manth@austin.utexas.edu

[**] This work was supported by Seven One Limited. We thank Thomas Cochell for his assistance with the XPS measurements and Karin M. Keller for the liquid chromatography analysis.

Supporting information for this article is available on the WWW under http://dx.doi.org/10.1002/anie.201301250.

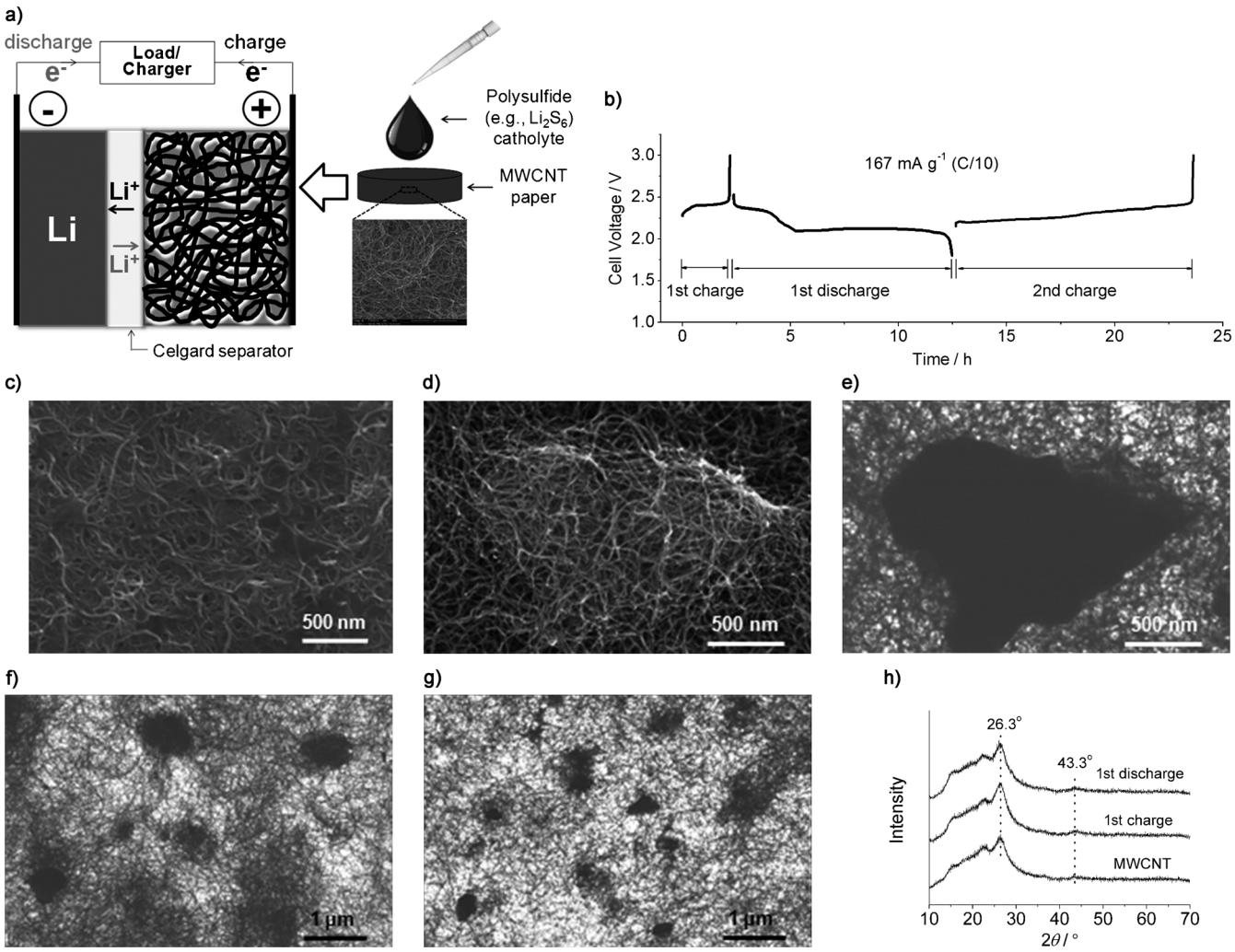

Figure 1. a) Schematic representation of the structure of a Li/dissolved polysulfide cell and the addition of polysulfide catholyte into a MWCNT electrode. b) Voltage versus time profile of the 1st charge, 1st discharge, and 2nd charge of the cell at C/10 rate. c) SEM image of the surface of a discharged MWCNT electrode. d) SEM image of a single particle wrapped by carbon nanotubes in the discharged MWCNT electrode. e) STEM image of the same area as in (d). f) STEM image of the charged MWCNT electrode. g) STEM image of the discharged MWCNT electrode. All the electrodes in (d), (e), (f), and (g) were washed with DME/DOL (1:1 v/v) solvent. h) XRD pattern of the pristine MWCNT paper, charged and discharged MWCNT electrodes.

MWCNT paper and cycled MWCNT electrodes after washing shows broad peaks at 2θ between 10 and 25°, which are attributed to the Kapton films covering the three samples. The sharp peak at $2\theta = 26.3°$ and the small peak at $2\theta = 43.3°$ correspond, respectively, to the (002) plane and (100) plane of graphitized MWCNTs.[9] Cycled MWCNT electrodes show almost identical patterns as the pristine MWCNT without any obvious peaks for elemental sulfur or Li_2S, indicating that the insoluble particles produced during charge and discharge exist in an amorphous state without long-range order. The low crystallinity of the charged and discharged products, which could be beneficial for reversible cathode reactions, is due to the presence of carbon nanotubes within the particles.

To identify the composition of the insoluble particles within the MWCNT network, cycled MWCNT electrodes before and after washing were analyzed by X-ray photoelectron spectroscopy (XPS). There are no obvious binding energy shifts among these four samples for the elements F 1s and C 1s (Figure S4 and S5), except for the decrease in peak intensity arising from the removal of $LiCF_3SO_3$ and electrolyte by washing. Figure 2a shows the S $2p_{1/2}$ and S $2p_{3/2}$ dual peaks with an intensity ratio of approximately 1:2 arising from spin orbit coupling. The peaks at 171.1 and 169.8 eV are only present before washing, and are characteristic of the soluble $LiCF_3SO_3$. The two strong peaks at low binding energies (161.9 and 160.4 eV) are only observed in the discharged MWCNT electrodes, and are assigned to Li_2S.[10] The peak intensities do not decrease after washing, indicating that the particles seen in Figure 1d, e, and g are insoluble Li_2S within the MWCNT network. Magnified peaks (×100) in the wavelength region between 167 and 162 eV are shown in Figure 2b. The small dual peaks at 165.1 and 163.8 eV are assigned to elemental sulfur. The weak peak intensities result likely from a negligible amount of elemental sulfur present on the electrode surface, suggesting the charged products are mainly within the electrode. These data indicate that ele-

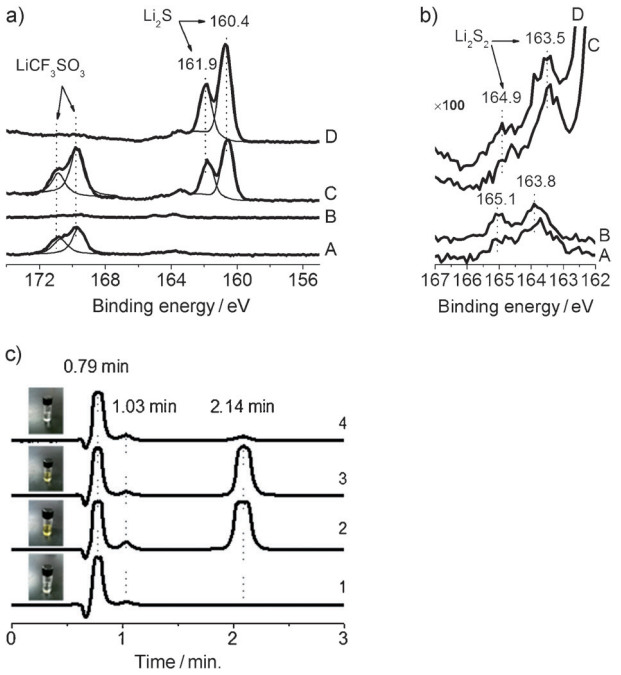

Figure 2. a) S 2p XPS spectra of the MWCNT electrodes: A) charged electrode without washing, B) charged electrode washed with electrolyte solvent, C) discharged electrode without washing, and D) discharged electrode washed with electrolyte solvent. b) Magnified (×100) XPS spectra of the same MWCNT electrodes as in (a) in the binding energy range of 167–162 eV. c) LC spectra and photographs of: 1) blank electrolyte, 2) polysulfide catholyte, 3) analyte after 1st charge, and 4) analyte after 1st discharge.

mental sulfur does form at the end of charge, which agrees with the recent results obtained with X-ray diffraction and transmission X-ray microscopy.[11] Two minor peaks at lower binding energies (164.9 and 163.5 eV) are observed for the discharged samples, which could be attributed to insoluble Li_2S_2,[10] an incomplete discharge product with a negligible amount.

To further analyze the products in the cycled cells, the washing solution after the treatment of all the parts within the cells was analyzed by liquid chromatography (LC). Figure 2c shows the LC spectra along with the photographs of blank electrolyte, polysulfide catholyte, analytes after the 1st charge and discharge. The blank electrolyte, a clear and transparent liquid, shows two peaks at retention times of 0.79 and 1.03 min which are attributed to the lithium salt and solvent. The third peak, at a retention time of 2.14 min in the yellow polysulfide catholyte, is a sign of the presence of polysulfides, which also appear in the analytes after the 1st charge (a strong peak) and discharge (a small peak). The color of the two analytes, as an indication of the polysulfide concentration, is also consistent with the peak intensities. These qualitative findings along with the XPS analysis support the conjecture that the charged catholyte contains soluble high-order polysulfides and the insoluble elemental sulfur is within the MWCNT electrode. In contrast, the discharge product in the form of insoluble Li_2S remains largely in the MWCNT electrode, leaving a negligible quantity of un-reacted polysulfides within the discharged catholyte.

Figure 3a shows the cyclic voltammograms of a Li/dissolved polysulfide cell. The potential was initially swept from the open circuit voltage (OCV) to 3.0 V followed by 10 cycles between 3.0 and 1.8 V at a rate of 0.1 $mV s^{-1}$. There are two cathodic peaks at 2.35 and 2.0 V corresponding to the reduction reactions of high order polysulfides and elemental sulfur, and two distinguishable anodic peaks in the anodic sweep which indicate clearly the staged transition of Li_2S to low-order polysulfides (e.g., Li_2S_4) and high-order polysulfides to elemental sulfur.[6b] The cell exhibits a very stable cycling profile without any noticeable decrease in peak intensity, revealing high reversibility of the cathode reactions during the 10 cycles except the initial sweep and 1st cycle. The overpotential observed in the initial sweep and the high-voltage cathodic peak in the first cycle indicate the occurrence of a conditioning process. Figure 3b shows voltage profiles of initial galvanostatic cycles at different rates. The cells exhibit high discharge capacities (based on the sulfur active mass within the catholyte used) of 1600 $mAh g^{-1}$, 1469 $mAh g^{-1}$, and 1261 $mAh g^{-1}$, respectively, at C/10, C/5, and C/2 rates. The capacities obtained correspond to more than 1.9 e^- per sulfur atom at C/10 and more than 1.5 e^- per sulfur atom at C/2. Figure 3c presents the extended cycling and Coulombic efficiency of these cells. Reversible capacities after 50 cycles remain high at 1411 $mAh g^{-1}$, 1317 $mAh g^{-1}$, and 1179 $mAh g^{-1}$ at the three rates. The capacities obtained are more than double those of the control Li/dissolved poly-

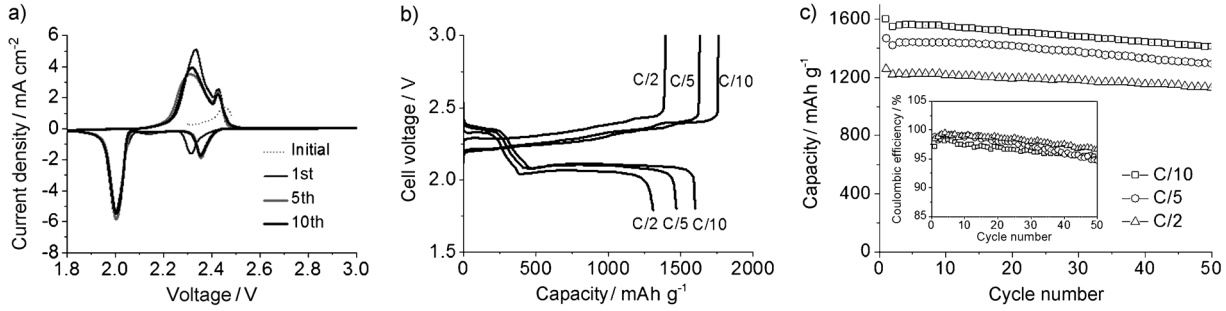

Figure 3. a) Cyclic voltammograms of a Li/dissolved polysulfide cell at a sweep rate of 0.1 $mV s^{-1}$ between 3.0 and 1.8 V including an initial sweep from the open circuit voltage to 3 V. b) Voltage versus specific discharge capacity profiles of initial galvanostatic cycles of Li/dissolved polysulfide cells at C/10, C/5, and C/2 rates. c) Cyclability of the cells at C/10, C/5, and C/2, where the capacity values are in terms of the sulfur active mass within the catholyte used (i.e., 1.9 mg sulfur or 1.7 $mg cm^{-2}$ sulfur). Inset: Coulombic efficiency of the cells.

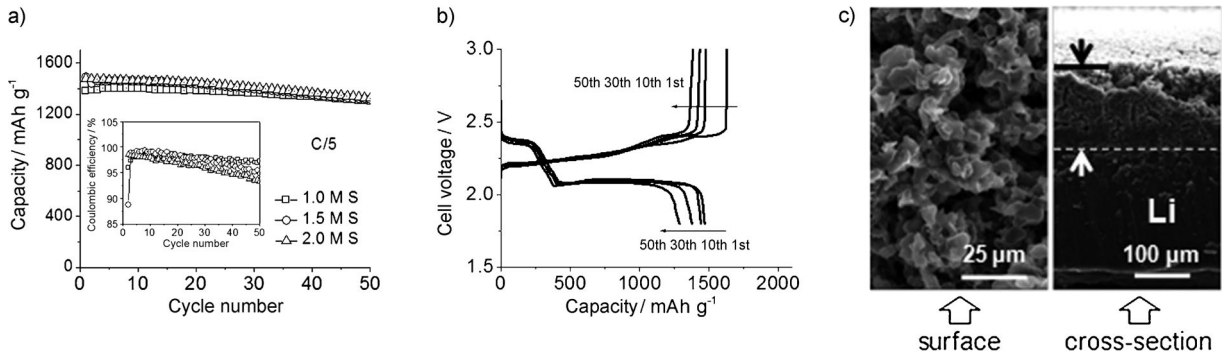

Figure 4. a) Cyclability of Li/dissolved polysulfide cells with different concentration (1.0, 1.5, and 2.0 M sulfur) of polysulfide catholytes at C/5 rate, where the capacity values are in terms of the sulfur active mass within the catholyte used. Inset: the Coulombic efficiency of the cells. b) Voltage versus specific discharge capacity profiles of the 1st, 10th, 30th, and 50th cycles with 1.5 M sulfur catholyte at C/5. c) SEM images of the surface (left) and cross-section (right) of a cycled lithium metal anode. The area between two arrows and lines in the cross-section SEM image indicates the passivation layer on the surface of the cycled lithium metal anode.

sulfide cell with Teflon-bonded Super P electrode and conventional sulfur electrodes (Figure S6). The Coulombic efficiency is over 95% with a degradation trend similar to that observed for the capacity. The capacity retention and Coulombic efficiency are higher under high-rate conditions because higher rate leads to a lower retention time of the dissolved polysulfides within the electrolyte per cycle, resulting in a suppression of the migration of polysulfides to the lithium anode side and a decrease in the loss of active material.

Figure 4a shows the cyclability of the cells with 1.0, 1.5, and 2.0 M sulfur catholyte at C/5 rate. Small differences in the discharge capacities, but large differences in Coulombic efficiency, are observed as a function of polysulfide concentration. Analogous to the sulfur-MWCNT composites, the sulfur contents within the MWCNT electrodes are 36, 46, and 53 wt.%, which are on par with the sulfur contents of other sulfur–carbon composites reported.[6a,c–h] The excellent reversibility of these cells with high capacities is because of the unique morphology of the intertwined MWCNT electrode architecture. The flexible carbon nanotubes intertwine together, forming the nanoscaled self-weaving, free-standing electrode. Upon cycling, the formation of solid products leads to an expansion of the MWCNT network, whereas the conversion of solid products into dissolved polysulfides leads to a contraction of interspaces between carbon nanotubes, maintaining the nanoscaled MWCNT electrode. The reversibility of the cathode reactions is sustained by the excellent flexibility and mechanical reversibility of the carbon nanotubes, as has been reported.[12] Cyclabilities of the cells with 1.0 and 2.0 M sulfur at 1C rate were also evaluated (Figure S7a). A stable capacity of around 1200 $mAh\,g^{-1}$ over 100 cycles at 1C rate was obtained with low concentration of sulfur (1 M). However, capacity fade was observed with high concentration of sulfur (2 M) at 1C rate. We believe the flexibility and mechanical reversibility of the carbon nanotubes at high rates under the conditions of densely deposited charged or discharged products with higher concentration of sulfur become restricted, resulting in poor electrochemical contact and low utilization of active material. To maintain good cyclability and high capacity, the Li/dissolved batteries with MWCNT electrodes need to be operated with an optimized concentration ($\leq$2 M sulfur) of polysulfide catholyte and at low or medium rates ($<$1C). With a higher concentration of sulfur (3 M) and higher sulfur content within the MWCNT electrode (62 wt.%), much lower capacities are obtained with a degradation of cycle life, as shown in Figure S7b. The density difference between sulfur (2.07 $g\,cm^{-3}$) and Li_2S (1.66 $g\,cm^{-3}$) results in a significant volume change during charge/discharge, requiring an optimized mass percentage (e.g., 30–60 wt.%) of sulfur within the MWCNT electrodes to maintain high capacity with good cyclability.

Figure 4b shows the 1st, 10th, 30th, and 50th charge and discharge voltage profiles of the cell with 1.5 M sulfur catholyte at C/5 rate. A slight decrease in discharge voltage is observed, and the discharge capacity decreases steadily with cycle number. The capacity loss is believed to be due to the continuous corrosion of the Li anode caused by the soluble polysulfides, which form a Li_2S/Li_2S_2 solid electrolyte interface film on the Li anode surface.[13] The SEM images in Figure 4c clearly show a thick passivation layer on the surface of a cycled lithium anode, which is rich in sulfur arising from the reaction between polysulfides and lithium resulting in the loss of active materials (Figure S8 and S9). After 50 cycles, the MWCNT electrode does not show a morphology change and there is not a passivation layer formed on the cycled MWCNT electrode (Figure S10). The capacity retention of the cells after resting in either charged or discharged state for one or two days was also evaluated and is shown in Figure S11. The cell in the discharged state retains over 92% of the initial capacity after 5 resting cycles, in contrast to less than 70% capacity retention for the cell in the charged state. The insoluble Li_2S formed within the carbon nanotube electrodes after discharge can reduce the loss of active material, whereas the soluble high-order polysulfides within the carbon nanotube electrode after charge can slowly diffuse to the lithium metal anode, causing capacity degradation. This result indicates that the Li/dissolved polysulfide cell should be kept in the discharged state to maintain a long shelf-life.

In summary, we have demonstrated highly reversible Li/dissolved polysulfide cells, utilizing an intertwined, free-

standing MWCNT paper as a host electrode. The high capacities obtained at rates of C/10, C/5, and C/2 are attributed to the unique MWCNT electrode architecture facilitating charge transport, formation of amorphous charge and discharge products, and the trapping of polysulfides and cycled products within the MWCNT electrode. This system offers a new way to solve the long-term reversibility obstacle facing rechargeable Li–S batteries and provides guidelines for designing electrode architectures and cell configurations to achieve high-energy-density batteries. The reversibility of the lithium-metal anode is becoming a predominant issue, which can be overcome by treating the lithium-metal-anode surface to suppress the contact with polysulfides or by development of solid-state electrolytes to eliminate the crossover of polysulfides. With these modifications, highly concentrated polysulfide catholytes could be used, which can improve the energy density of Li/dissolved polysulfide cells for portable electronic and stationary energy-storage applications.

Experimental Section

To fabricate the self-weaving, free-standing MWCNT paper commercial MWCNTs (75 mg) synthesized by a chemical vapor deposition process were dispersed in de-ionized water (750 mL) by high-power ultrasonication for 15 min with the addition of isopropyl alcohol (20 mL) to wet the MWCNTs. The products were collected by vacuum filtration and washed with de-ionized water, ethanol, and acetone several times. The free-standing MWCNT paper thus formed was a flexible film after drying for 24 h at 100 °C in an air-oven, which could be easily peeled off the filter membrane. The MWCNT paper was then punched out in circular disks with 1.2 cm diameter (1.13 cm^2), 40–50 micron thickness, and 1.9–2.3 mg mass. In the control experiment, a Super P carbon electrode was prepared by mixing Super P carbon and polytetrafluoroethylene (PTFE) in a weight ratio of 3:2 in a mortar with isopropyl alcohol as a dispersing agent. The mixture was then pressed and cut into disks with the same size as the MWCNT electrodes. The Super P electrodes were dried at 100 °C in an air oven before assembling the cell. Blank electrolyte was prepared by dissolving the appropriate amount of lithium trifluoromethanesulfonate ($LiCF_3SO_3$, 98%, Acros Organics) and lithium nitrate ($LiNO_3$, 99+%, Acros Organics) in a dimethoxy ethane (DME, 99+%, Acros Organics) and 1,3-dioxolane (DOL, 99.5%, Acros Organics) (1:1 v/v) mixture solvent to give a 1 M $LiCF_3SO_3$ and 0.1 M $LiNO_3$ solution. To prepare the dissolved polysulfide catholyte, sublimed sulfur powder (99.5%, Acros Organics) and an appropriate amount of lithium sulfide (Li_2S, 99.9%, Acros Organics) were added to the proper amount of blank electrolyte to give 1.0 M, 1.5 M, 2.0 M, and 3.0 M sulfur in the form of Li_2S_6 in the solution. The mixture solution was heated at 45 °C in an Ar-filled glove box for 18 h to produce a dark yellow solution with moderate viscosity.

Li/dissolved polysulfide cells (CR2032 coin cells) were assembled in an Ar-filled glove box. First, polysulfide catholyte (40 μL) was added into the MWCNT paper electrode, corresponding to 1.3 mg (1.2 mg cm^{-2}), 1.9 mg (1.7 mg cm^{-2}), and 2.6 mg (2.3 mg cm^{-2}) of sulfur, respectively, for the 1.0, 1.5, and 2.0 M sulfur catholytes. Then a Celgard 2400 separator was placed on the top of the MWCNT electrode. blank electrolyte (20 μL) was added on the separator followed by, respectively, another separator and blank electrolyte (20 μL). Finally, the lithium metal anode was placed on the separator. In the control experiment, Super P electrode was used. A conventional Li–S cell was also fabricated and tested for a comparison. The sulfur cathode was prepared by mixing ground sulfur powder (60 wt.%), Super P carbon (20 wt.%), and poly(vinylidene difluoride) (PVdF) binder (20 wt.%), and dispersing the mixture in *N*-methylpyrrolidone (NMP, 99%, Acros Organics) overnight to prepare a slurry. The slurry was then cast onto an aluminum foil current collector, followed by evaporating the NMP at 50 °C under a flowing air oven for 24 h. The sulfur electrode was then punched out in circular disks with 1.2 cm diameter, 40–50 micron thickness, and 1.0–1.2 mg sulfur active material. The conventional Li–S cells were also assembled in the Ar-filled glove box. First, blank electrolyte (20 μL) without polysulfide was added onto the sulfur electrode. Then a Celgard separator was placed on top of the electrode, followed by the addition of blank electrolyte (20 μL) on the separator and lithium metal anode.

Morphological characterizations were carried out with a FEI Quanta 650 scanning electron microscope (SEM) and a Hitachi S-5500 SEM equipped with a scanning transmission electron microscope (STEM). The elemental mapping results were examined with an energy dispersive spectrometer (EDS) attached to the FEI Quanta 650 SEM. The XRD data were collected on a Philips X-ray diffractometer equipped with CuKα radiation in steps of 0.02°. XRD samples were covered by Kapton films in an Ar-filled glove box. X-ray photoelectron spectroscopy (XPS) data were collected at room temperature with a Kratos Analytical spectrometer and monochromatic $Al_{K\alpha}$ (1486.6 eV) X-ray source. Cycled cells, either 1st charged or 1st discharged, were opened in the Ar-filled glove box. The cycled MWCNT electrodes were taken for SEM, XRD, and XPS measurements. Some cycled MWCNT electrodes were washed with DME/DOL (1:1 v/v) solvent thoroughly for SEM, STEM, and XPS measurements. Liquid chromatography (LC) data were acquired on a Dionex Ultimate 3000 HPLC system. All parts of the cycled cells including lithium metal anode, separator, coin cell components, and MWCNT electrodes were washed with DME/DOL (10 mL; 1:1 v/v) solvent as analytes. Blank electrolyte (40 μL) and polysulfide catholyte were diluted with DME/DOL (10 mL; 1:1 v/v) solvent for a comparison. An aliquot of each sample was injected onto a Phenomenex Gemini C18 column (5 micron, 2 × 50 mm) and eluted with 100% methanol at a flow rate of 0.2 mL min^{-1}. UV detection was performed at 254 nm.

Cyclic voltammetry data were collected with a VoltaLab PGZ402 with an assembled coin cell between 1.8 and 3.0 V at a scan rate of 0.1 mV s^{-1}. Electrochemical performances of the coin cells were galvanostatically evaluated with an Arbin battery test station between 1.8 and 3.0 V at various C rates. The cells for the characterization and electrochemical evaluation contain 1.5 M sulfur catholyte except in those indicated. The capacity values shown in this paper are calculated by dividing the capacities obtained by the mass of sulfur within the catholyte used or within the conventional electrodes. The capacity retention of cells after resting for a period of time was evaluated by measuring the discharge capacity after the cell was rested in the charged state for one or two days and then discharging to 1.8 V at C/10 rate or after the cell was rested in the discharged state for two days and then charging to 3.0 V at C/10 rate.

Received: February 12, 2013
Revised: March 28, 2013
Published online: May 29, 2013

Keywords: carbon nanotubes · electrochemistry · electrode materials · lithium–sulfur battery · polysulfide catholyte

[1] a) P. G. Bruce, S. A. Freunberger, L. J. Hardwick, J.-M. Tarascon, *Nat. Mater.* **2012**, *11*, 19–29; b) X. Ji, L. F. Nazar, *J. Mater. Chem.* **2010**, *20*, 9821–9826.

[2] a) R. D. Rauh, K. M. Abraham, G. F. Pearson, J. K. Surprenant, S. B. Brummer, *J. Electrochem. Soc.* **1979**, *126*, 523–527; b) H. Yamin, E. Peled, *J. Power Sources* **1983**, *9*, 281–287.

[3] a) Y. V. Mikhaylik, J. R. Akridge, *J. Electrochem. Soc.* **2004**, *151*, A1969 – A1976; b) J. R. Akridge, Y. V. Mikhaylik, N. White, *Solid State Ionics* **2004**, *175*, 243 – 245.
[4] C. Barchasz, F. Molton, C. Duboc, J.-C. Leprêtre, S. Patoux, F. Alloin, *Anal. Chem.* **2012**, *84*, 3973 – 3980.
[5] a) J. Shim, K. A. Striebel, E. J. Cairns, *J. Electrochem. Soc.* **2002**, *149*, A1321 – A1325; b) S.-E. Cheon, K.-S. Ko, J.-H. Cho, S.-W. Kim, E.-Y. Chin, H.-T. Kim, *J. Electrochem. Soc.* **2003**, *150*, A800 – A805; c) C. Liang, N. J. Dudney, J. Y. Howe, *Chem. Mater.* **2009**, *21*, 4724 – 4730; d) C. Lai, X. P. Gao, B. Zhang, T. Y. Yan, Z. Zhou, *J. Phys. Chem. C* **2009**, *113*, 4712 – 4716.
[6] a) X. Ji, K. T. Lee, L. F. Nazar, *Nat. Mater.* **2009**, *8*, 500 – 506; b) N. Jayaprakash, J. Shen, S. S. Moganty, A. Corona, L. A. Archer, *Angew. Chem.* **2011**, *123*, 6026 – 6030; *Angew. Chem. Int. Ed.* **2011**, *50*, 5904 – 5908; c) R. Elazari, G. Salitra, A. Garsuch, A. Panchenko, D. Aurbach, *Adv. Mater.* **2011**, *23*, 5641 – 5644; d) R. Demir-Cakan, M. Morcrette, F. Nouar, C. Davoisne, T. Devic, D. Gonbeau, R. Dominko, C. Serre, G. Férey, J.-M. Tarascon, *J. Am. Chem. Soc.* **2011**, *133*, 16154 – 16160; e) L. Ji, M. Rao, H. Zheng, L. Zhang, Y. Li, W. Duan, J. Guo, E. J. Cairns, Y. Zhang, *J. Am. Chem. Soc.* **2011**, *133*, 18522 – 18525; f) G. Zheng, Y. Yang, J. J. Cha, S. S. Hong, Y. Cui, *Nano Lett.* **2011**, *11*, 4462 – 4467; g) C. Zhang, H. B. Wu, C. Yuan, Z. Guo, X. W. Lou, *Angew. Chem.* **2012**, *124*, 9730 – 9733; *Angew. Chem. Int. Ed.* **2012**, *51*, 9592 – 9595; h) Y.-S. Su, A. Manthiram, *Chem. Commun.* **2012**, *48*, 8817 – 8819.
[7] a) C. Barchasz, F. Mesguich, J. Dijon, J.-C. Leprêtre, S. Patoux, F. Alloin, *J. Power Sources* **2012**, *211*, 19 – 26; b) R. Demir-Cakan, M. Morcrette, B. Gangulibabu, A. Guéguen, R. Dedryvère, J.-M. Tarascon, *Energy Environ. Sci.* **2013**, *6*, 176 – 182; c) R. Xu, I. Belharouak, J. C. M. Li, X. Zhang, I. Bloom, J. Bareño, *Adv. Energy Mater.* **2013**, DOI: 10.1002/aenm.201200990.
[8] S. Y. Chew, S. H. Ng, J. Wang, P. Novák, F. Krumeich, S. L. Chou, J. Chen, H. K. Liu, *Carbon* **2009**, *47*, 2976 – 2983.
[9] F. Wang, S. Arai, M. Endo, *Carbon* **2005**, *43*, 1716 – 1721.
[10] H. Ota, T. Akai, H. Namita, S. Yamaguchi, M. Nomura, *J. Power Sources* **2003**, *119 – 121*, 567 – 571.
[11] J. Nelson, S. Misra, Y. Yang, A. Jackson, Y. Liu, H. Wang, H. Dai, J. C. Andrews, Y. Cui, M. F. Toney, *J. Am. Chem. Soc.* **2012**, *134*, 6337 – 6343.
[12] A. Cao, P. L. Dickrell, W. G. Sawyer, M. N. Ghasemi-Nejhad, P. M. Ajayan, *Science* **2005**, *310*, 1307 – 1310.
[13] N.-S. Choi, Z. Chen, S. A. Freunberger, X. Ji, Y.-K. Sun, K. Amine, G. Yushin, L. F. Nazar, J. Cho, P. G. Bruce, *Angew. Chem.* **2012**, *124*, 10134 – 10166; *Angew. Chem. Int. Ed.* **2012**, *51*, 9994 – 10024.

